RESEARCH ARTICLE

WILEY

Rationally designed graphene channels for real-time sodium ion detection for electronic tongue

Chung Won Lee[1] | **Sang Eon Jun**[1] | **Seung Ju Kim**[1] | **Tae Hyung Lee**[1] | **Sol A. Lee**[1] | **Jin Wook Yang**[1] | **Jin Hyuk Cho**[2] | **Shinyoung Choi**[3] | **Cheol-joo Kim**[3] | **Soo Young Kim**[2] | **Ho Won Jang**[1,4] ⓘ

[1]Department of Materials Science and Engineering, Research Institute of Advanced Materials, Seoul National University, Seoul, Republic of Korea

[2]Department of Materials Science and Engineering, Korea University, Seoul, Republic of Korea

[3]Department of Chemical Engineering, Pohang University of Science and Technology (POSTECH), Pohang, Republic of Korea

[4]Advanced Institute of Convergence Technology, Seoul National University, Suwon, Republic of Korea

Correspondence
Cheol-joo Kim, Department of Chemical Engineering, Pohang University of Science and Technology (POSTECH), Pohang 37673, Republic of Korea.
Email: kimcj@postech.ac.kr

Soo Young Kim, Department of Materials Science and Engineering, Korea University, 145 Anam-ro, Seongbuk-gu, Seoul 02841, Republic of Korea.
Email: sooyoungkim@korea.ac.kr

Ho Won Jang, Department of Materials Science and Engineering, Research Institute of Advanced Materials, Seoul National University, Seoul 08826, Republic of Korea.
Email: hwjang@snu.ac.kr

Abstract

Monitoring taste-inducing ions and molecules continuously in liquids or solutions is of great considerable matter for the realization of the electronic tongue (E-tongue). Particularly from the five major tastes, the highly selective, sensitive detection of Na^+ in real-time is prioritized. Prioritization is due to the saltiness of food is the key ingredient in most meals. Nevertheless, existing Na^+ detecting devices have relatively low performances of selectivity, sensitivity, and lack of on–off functions. Additionally, conventional devices significantly deteriorate in capacity due to repetitive usage or lifetime shortage by degradation of the sensing material. Herein, a graphene-based channel was rationally designed by the facile decoration of Calix[4]arene and Nafion to address this issue. They act as a receptor and a molecular sieve, respectively, to enhance selectivity and sensitivity and elongate the life expectancy of the device. This device was merged with a microfluidic channel to control the injection and withdrawal of solutions to fulfill dynamic on–off functions. The fabricated device has highly selective, sensitive Na^+ detection properties compared to other 10 molecule/ionic species. Dynamic on–off functions of the device were available, also possesses a long lifespan of at least 220 days. Additionally, it can precisely discriminate real beverages containing Na^+, which can be observed by principal component analysis plot. These features offer the possibility of ascending to a platform for E-tongues in near future.

KEYWORDS

electronic tongue, graphene, microfluidic channels, Na^+ sensors, solution-gated field-effect transistors

1 | INTRODUCTION

The necessity for monitoring food salinity has recently led to considerable interest in daily life. Detecting the amount of salt is much more crucial than other factors of food monitoring since it is directly related to severe diseases or even death. Excessive salt intake induces cardiovascular diseases, stroke, kidney malfunction, and so on.[1] On the other hand, the lack of salt consumption causes hyponatremia (shortage of salt in blood), and if this state continues, muscle cramps, nausea, vomiting, and dizziness occurs.[2] Moreover, due to the "COVID-19" pandemic, many people try to consume food by cooking rather than eating out.[3] However, the recipes differ because the appetite varies, and subjective recipes may mislead people into excessive salt consumption. According to WHO (World Health Organization), people consume more salt than the recommended amount (about 2 g of sodium daily is recommended).[4] Despite the increased demand for cooking at home, consumers are ignorant of the suggested daily amount of salt, causing more sodium intake. Real-time monitoring sensors that detect the absolute quantity of salt possess prominent standards and recognize consumers. Due to this, an intuitive, real-time monitoring device of salinity in food is vital. However, due to their high cost and portability issues, traditional E-tongues are inapplicable for monitoring the taste or freshness of food in real-time. To check the salinity of food in real life, the E-tongue must be portable and have unique functions of monitoring salt or sodium in real-time. Therefore, the evolution of a simple, miniaturized, low-cost, high-performed E-tongue is important to address the desire to evade an unhealthy diet containing excessive salt.

The choice of materials for the E-tongue is crucial because it affects the performance of the sensor unit. The performance of the E-tongue is estimated by detecting minuscule changes in the concentration of particular ions or molecules.[5,6] Metallic electrodes,[7] lipid membranes,[8] conducting polymers,[9] and two dimensional (2D) materials[10,11] are typical candidates for the E-tongue. Above all, many researchers have been conducting sensing applications of ionic and molecular species in liquid using 2D materials, such as graphene, MoS_2, and other transitional metal dichalcogenides (TMDs), for various reasons. The chemical and physical properties of 2D materials make them appropriate for application in sensing devices. The high surface-area-to-volume ratio of 2D materials provides high sensitivity to ions and molecules.[10,12] Additionally, strong mechanical strength, flexibility, and transparency make it possible to minimize the sensing device. 2D materials generally have the features mentioned above; especially graphene has

characteristics that differ from those of others. For example, in terms of conductivity properties, graphene is semi-metallic because it has a zero bandgap[13] and graphene SFETs exhibit bipolar characteristics.[14]

Graphene outstands other candidates from these benefits of 2D materials, realizing a simple, miniaturized, low-cost, and high-performed E-tongue. Due to these advantages, numerous types of research based on ion/molecular sensors using 2D materials, particularly graphene,[6,15–17] were conducted, and devices were developed; yet possessing limitations such as the lack of a dynamic on–off function and low selectivity. The most noticeable feature of previous studies based on ion/molecular sensors includes one-sided amperometric sensor curves.[18,19] These sensing curves cannot prove the reversibility of the device due to the absence of a standard or base resistance/current. Irreversibility is from the unavailability of ejection of the injected solutions that influence the baseline. Repeatability and reliability are also indispensable factors, as well as high selectivity and sensitivity to satisfy the sensor conditions. However, existing amperometric sensing curves have a one-sided upward or downward shape, which cannot demonstrate repeatability or reliability.[18,19] The successive addition of the following solution without discharging the previous one causes a monotonic increase/decrease of resistance or conductivity baseline from the amperometric data. The baseline current fluctuates when a new solution flows into the device without discharging the remaining. However, current baseline consistency is necessary for reliable and repeatable ion/molecule detection evaluations. The reliability and repeatability are maintained by discarding the redundant solution and injecting a washing solution simultaneously. The washing solution can be used with deionized water (DI) or NaOH. The target ion/molecule must be dissolved in the same solution or electrolyte chosen as the washing solution. The merge of a microfluidic channel with the graphene-based FET leads to simultaneous and repetitive injection/withdrawal of solutions. The integrated device allows solutions to flow dynamically and creates an alternative base and response current in a sequence. The repetitive response and baseline curves can be assumed "on" and "off." This dynamic on–off function allows real-time detection of ion/molecule species. Real-time detection is acquired by comparing the response, and base current intensity ratio as the solution flows in and out through the SFET device. To conclude, integrating a novel designed microfluidic channel with the graphene-based FET results in simultaneous and repetitive injection/withdrawal of solutions leading to dynamic on–off functions. This provides the graphene-based SFET device to detect target solutions in real-time reliably and repetitively.

In this study, we conceive an ion/molecule sensor based on graphene, which is selective and sensitive to Na^+, using single steps of coating or decoration. Our research shows the potential of the Nafion membrane, which is spin-coated, and selectively allows Na^+ or small cations to permeate through the membrane, acting as a
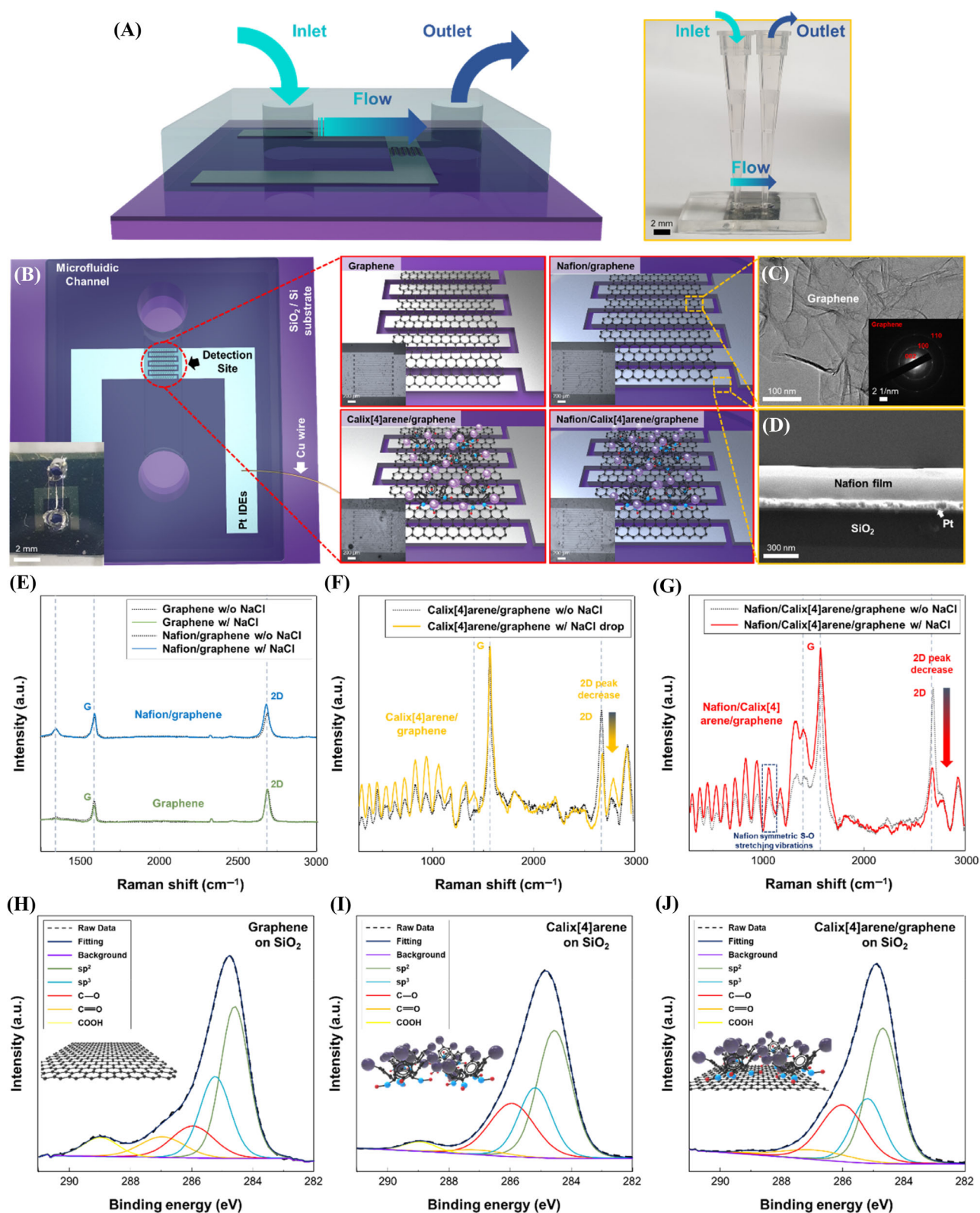

FIGURE 1 Legend on next page.

molecular sieve.[6,20–22] Calix[4]arene, known as a receptor of Na^+, is decorated by drop-casting onto the surface of graphene, showing high sensitivity.[23,24] Also, dynamic on–off functions are available by introducing the novel designed microfluidic channel onto the graphene-based FET, producing reversible and reliable sensing curves. Due to the on–off functions, detection curves are intuitively compared, and the sensitivity can be easily noticed in a specific dissolved ion/molecule solution. Chemical solutions and beverages were used to evaluate the performance of the graphene-based SFET for practical usage. Furthermore, the beverage detection data were estimated using principal component analysis (PCA) to differentiate the drinks intuitively. These results prove that the fabricated graphene-based SFET device can reliably and selectively detect Na^+, and the capacity of differing real beverages demonstrates the potential for application as an E-tongue.

2 | RESULTS AND DISCUSSION

2.1 | Sensor design and analysis of graphene, Nafion/graphene, and Calix[4]arene/graphene

By using the chemical vapor deposition (CVD) process, single-layered graphene was transferred to an IDE. (Figure S1a) After the transferring process, the samples were classified into four groups having different additional steps; Graphene, Nafion/graphene, Calix[4]arene/graphene, and Nafion/Calix[4]arene/graphene. (Figure 1B) The overall sample fabrication process is illustrated in Figure S1b. After transferring single-layered pristine graphene (step 1) on the IDE, Calix[4]arene dispersed in *N,N*-dimethylformamide (DMF) was drop-casted onto the site (step 2). Then, the Nafion solution was spin-coated onto the IDE sample (step 3). Patterned polydimethylsiloxane (PDMS) was attached to the IDE sample forming a microfluidic channel system (step 4). The other samples were fabricated by the following process; a pristine graphene sample was made by transferring single-layered pristine graphene (step 1) and then attaching the patterned PDMS (step 4). The Nafion/graphene sample was fabricated by transferring graphene (step 1), directly spin-coating the Nafion solution onto the sample (step 3), and finally attaching the patterned PDMS (step 4). Calix[4]arene/graphene sample was made by transferring graphene (step 1), drop-casting Calix[4]arene onto the IDE (step 2), and adhering to the patterned PDMS (step 4). The scheme and image of the fabricated device are depicted in Figure 1A. The solution or liquid flow is presented in the figure.

As mentioned above, flow control leads to dynamic on–off functions, crucial for conspicuous, objective datasets. Sodium selectivity is achieved by coating Nafion, which prevents the penetration of large molecules or ions, and decorating Calix[4]arene acts as a sodium ion receptor. The Nafion-coated membrane blocks large taste-inducing molecules or ions from being adjacent to the surface of the graphene. The Nafion membrane only lets single ions penetrate, such as H^+, Na^+, K^+, Mg^{2+}, Ca^{2+}, and NH_4^+.[20,21,25–27] The Nafion membrane itself has insufficient selectivity for measuring Na^+, indicating that a receptor is needed. However, by the identical cavity size of Calix[4]arene and the diameter of Na^{+}[28] and attraction between Na^+ with the O from Calix[4]arene,[29–31] the selectivity of Na^+ is enhanced thoroughly. Analyzing the existence and morphologies of the Nafion membrane and clarifying the relationship between Na^+ and Calix[4]arene is crucial to revealing the sensing properties. The scheme and optical microscopy (OM) images of the samples on the IDE are shown in Figure 1B, transmission electron microscopy (TEM) images are depicted in Figure 1C, and a cross-sectional scanning electron microscopy (SEM) image is shown in Figure 1D. The microfluidic channel merged IDE scheme is displayed, showing the real image on the inset. The magnified region of the detection site is depicted on the right, showing the four different samples and how graphene, Calix[4]arene, and Nafion are transferred, decorated or coated. The OM images of the detection site are displayed on the insets of each sample.

Figure 1C depicts the graphene transferred on a Cu grid obtained by TEM, which can be noticed by the wrinkles.[32] The inset shows the selected area electron diffraction (SAED) patterns of the transferred graphene. The polycrystalline rings of graphene 002, 100, and 110 were

FIGURE 1 Device structure and characterization of graphene, Nafion/graphene, Calix[4]arene/graphene, and Nafion/Calix[4]arene/graphene by OM, TEM, SEM, Raman spectroscopy, and XPS. (A) The overall scheme and image of the fabricated device integrated with a microfluidic channel showing flow directions of the solution. (B) Scheme and OM of the device, Pristine graphene, Nafion/graphene, Calix[4]arene/graphene, and Nafion/Calix[4]arene/graphene. (C) TEM image of the graphene. The inset shows the SAED patterns of the produced graphene. (D) Cross-sectional SEM image of Nafion/graphene. (E) Raman spectroscopy of graphene and Nafion/graphene with and without Na^+. (F,G) Raman spectroscopy of Calix[4]arene/graphene and Calix[4]arene/Nafion decorated graphene with and without Na^+. (H–J) XPS C 1s spectra of graphene, Calix[4]arene, and Calix[4]arene/graphene.

obtained.[6] A cross-sectional SEM image is depicted in Figure 1D to determine the thickness of the Nafion-coated film.[33] The thickness of the membrane is approximately 280 nm, estimated from the bright region, and it can be assumed that large molecules or ions cannot penetrate due to their density.[6]

The analysis and scheme of Raman spectra measurement of graphene, Nafion/graphene, Calix[4]arene/graphene, and Nafion/Calix[4]arene/graphene samples are displayed in Figure S2. To reveal the influence of Na^+, the Raman peaks of all four samples were measured in the air without any treatments. Then peaks were estimated after dropping and drying 100 µL of 10 mM NaCl onto the identical samples, which were evaluated in air conditions. The samples were dried on a 70°C hotplate until the water evaporated. All four samples have unique characteristics by the existence of Nafion, Calix[4]arene, and Na^+. Figure 1E shows the results of the Raman spectra, which can be assumed that the CVD graphene is single-layered and relatively free of defects by the lack of the D peak.[34] On the other hand, Nafion/graphene and Nafion/Calix[4]arene/graphene have a significant peak compared to CVD graphene at 1350 cm^{-1}. The low-intensity turbulent peaks below the wavelength 1350 cm^{-1} in Figure 1F,G shows the peaks from Calix[4]arene.[35] In Figure 1E,G, this peak might be assumed as a D peak, but there are reports of appearing the D peak on CVD graphene when coated with Nafion.[36] This is difficult to distinguish with the peak of the Nafion alone,[36] intending that the graphene has a low level of defects. As depicted in Figure 1E, in both CVD graphene and Nafion/graphene cases, the Raman peaks were identical to the samples dropped or not with NaCl solution. On the other hand, the Raman peaks of Calix[4]arene/graphene and Nafion/Calix[4]arene/graphene differ from the samples which were dropped or not with the solution. Figure 1F,G shows that the G peak has an identical intensity in all cases; the 2D peak decreases conspicuously when the NaCl solution is dropped and dried on the sample. From other research, the intensity ratio of Raman peaks between G and 2D (noted as I(G)/I(2D)) increase intends the doping state of graphene.[37] The intensity of the G peak is independent of the doping state, but the 2D peak strongly declines with increasing doping. Comparing the samples dropped with NaCl and dried, the presence or absence of Calix[4]arene (receptor) shows a conspicuous difference in the 2D peak intensity decrease. This assumes that Calix[4]arene acts as a crucial factor in the case of detecting Na^+ selectively and sensitively. Nafion also has peak changes while Na^+ penetrates through the membrane. Since the cations or water molecules interact with the SO_3^-, the symmetric S-O stretching vibrations may change during transportation.[38–42] The peak intensity from SO_3^- increased conspicuously as Na^+ dried in Figure 1G.

In conclusion, CVD graphene itself does not adsorb Na^+ thoroughly. In contrast, Calix[4]arene/graphene highly draws Na^+ due to the existence of the receptor shown by the magnificent decrease of the Raman 2D peak and the change of doping state. The graphene becomes n-doped when Na^+ becomes adjacent to the graphene surface (the n-doping degree is much higher when Calix[4]arene is decorated).[43–45] The exact mechanism and reason for Na^+ adhesion rather than Cl^- will be explained later.

X-ray photoelectron spectroscopy (XPS) was also carried out to reveal the existence of Calix[4]arene on the graphene, and Fourier transform infrared (FTIR) spectra of Calix[4]arene is depicted in Figure S3d. The XPS survey scan of graphene, Calix[4]arene, and Calix[4]arene/graphene are displayed in Figure S3a–c. For clearer comparison, high-resolution XPS C 1s spectra of graphene, Calix[4]arene, and Calix[4]arene/graphene was displayed in Figure S1h–j. All three samples of C 1s peaks were recorded, and from the deconvolution, C=C (sp^2), C—C (sp^3), C—O, C=O, and COOH existed. The binding energies of graphene were; C=C (284.6 eV), C—C (285.2 eV), C—O (286 eV), C=O (287 eV), COOH (289 eV), Calix[4]arene were; C=C (284.5 eV), C—C (285.1 eV), C—O (285.9 eV), C=O (287 eV), COOH (288.9 eV), and Calix[4]arene/graphene were; C=C (284.6 eV), C—C (285.1 eV), C—O (286 eV), C=O (286.9 eV), COOH (289 eV). These C 1s binding energy values correspond to previous studies.[46–48] Comparing C—O bonding between the samples is the most reasonable method to discriminate the materials since Calix[4]arene has C—O bonding from the frame. In contrast, graphene does not have C—O bonding theoretically. However, due to contamination, graphene has low level of C—C, C—O, C=O, and COOH bonds.[49–52] According to Figure 1H,I, the C—O bonding peak intensity level is conspicuously discretized that even considering Calix[4]arene might have been contaminated, C—O bonding exists from the frame.[53] Furthermore, comparing Figure 1H,I, the contamination level of Calix[4]arene is much lower than graphene as the peaks of C=O and COOH are minuscule. Figure 1J displays similar results to Figure 1I, as Calix[4]arene is decorated onto the graphene. The results are reasonable, considering the XPS survey is a surface chemistry analysis method. Additionally, Figure S3d shows Fourier transform infrared (FTIR) spectra of Calix[4]arene, which was measured to verify the existence of the material.

2.2 | Na^+ detection performance of the four graphene SFETs

Graphene, Nafion/graphene, Calix[4]arene/graphene, and Nafion/Calix[4]arene/graphene were exposed to
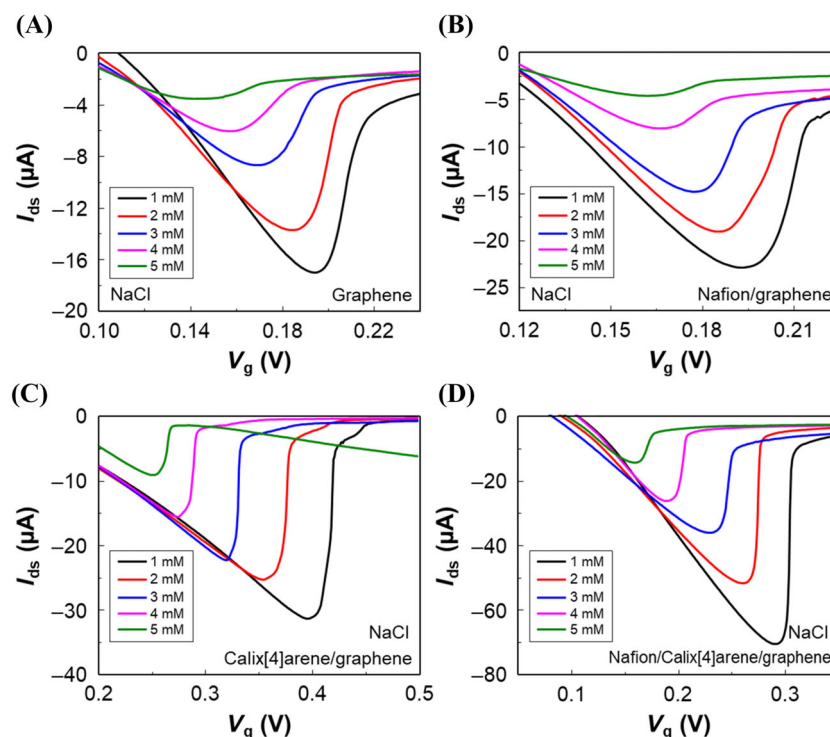
FIGURE 2 Transfer characteristics of graphene, Nafion/graphene, Calix[4]arene/graphene, and Nafion/Calix[4]arene/graphene. Na^+ transfer curves of (A) graphene (B) Nafion/graphene (C) Calix[4]arene/graphene (D) Nafion/Calix[4]arene/graphene ranging from 1 to 5 mM.

various NaCl solution concentrations and analyzed. The transfer characteristics and detection properties of the four graphene SFETs were estimated. Also, other ions and molecules, including H^+, citric acid, KCl, $CaCl_2$, $MgCl_2$, NH_4Cl, glutamic acid, ascorbic acid, glucose, and uric acid, were tested for comparison of selectivity and sensitivity of the four graphene SFETs.

Figure 2A–D illustrates the transfer characteristics of graphene, Nafion/graphene, Calix[4]arene/graphene, and Nafion/Calix[4]arene/graphene. The transfer characteristics were evaluated by changing the gate voltage (V_g) over the source-drain current (I_{ds}). The charge transport properties of the graphene-based SFETs can be investigated by shifting the Dirac point with various electrolytes. The ambipolar features of graphene cause n- or p-doping effects in the graphene layer when the solution-gated graphene channel is modulated by accumulated ions (electrons or holes).[54] Additionally, compared to other 2D materials, the $I–V$ characteristics of graphene reveal a unique "U-shape" due to its ambipolar feature.[14] Setting the reference point as the Dirac point (the local minimum point of the $I–V$ curve), the left region has hole conduction, while the right region has electron conduction.[14] This indicates that both hole and electron participate in the conductivity of graphene.

All four graphene-based SFETs have the same shifting aspects (x-axis decrement) by the NaCl solution concentration elevation. Also, the minimum conductivity variation (y-axis increment, i.e., a decrease of the absolute value) features have the same tendency. The difference between CVD graphene, Nafion/graphene, and Calix[4]arene/graphene, Nafion/Calix[4]arene/graphene, respectively, have relatively small deviations in both cases of V_g and I_{ds}. Calix[4]arene influences the Dirac point shift (V_g) and minimum conductivity variation (I_{ds}) because it acts as a Na^+ receptor causing more value divergence between different solutions. Figure 2A–D provides information on the four samples of V_g and I_{ds} shift between 1 and 5 mM NaCl solutions. CVD graphene approximately shifted $|V_g| = 0.05$ V, $|I_{ds}| = 13.6$ µA, Nafion/graphene shifted $|V_g| = 0.032$ V, $|I_{ds}| = 18.4$ µA, Calix[4]arene/graphene shifted $|V_g| = 0.145$ V, $|I_{ds}| = 21.8$ µA, Nafion/Calix[4]arene/graphene shifted $|V_g| = 0.133$ V, $|I_{ds}| = 56.9$ µA.

The degree and direction of the Dirac point shift determine the transfer characteristics. Figure 2A–D shows a left shift as the concentration of NaCl solution increases. This suggests that the graphene-based SFETs become n-doped as NaCl concentration increases. The position of the Dirac point evaluates the doping state and degree.[14] As the graph moves to the left, the applied V_g relatively becomes positioned further to the right. Since the type and density of the carrier are decided by the difference between the channel and gate, a relatively larger
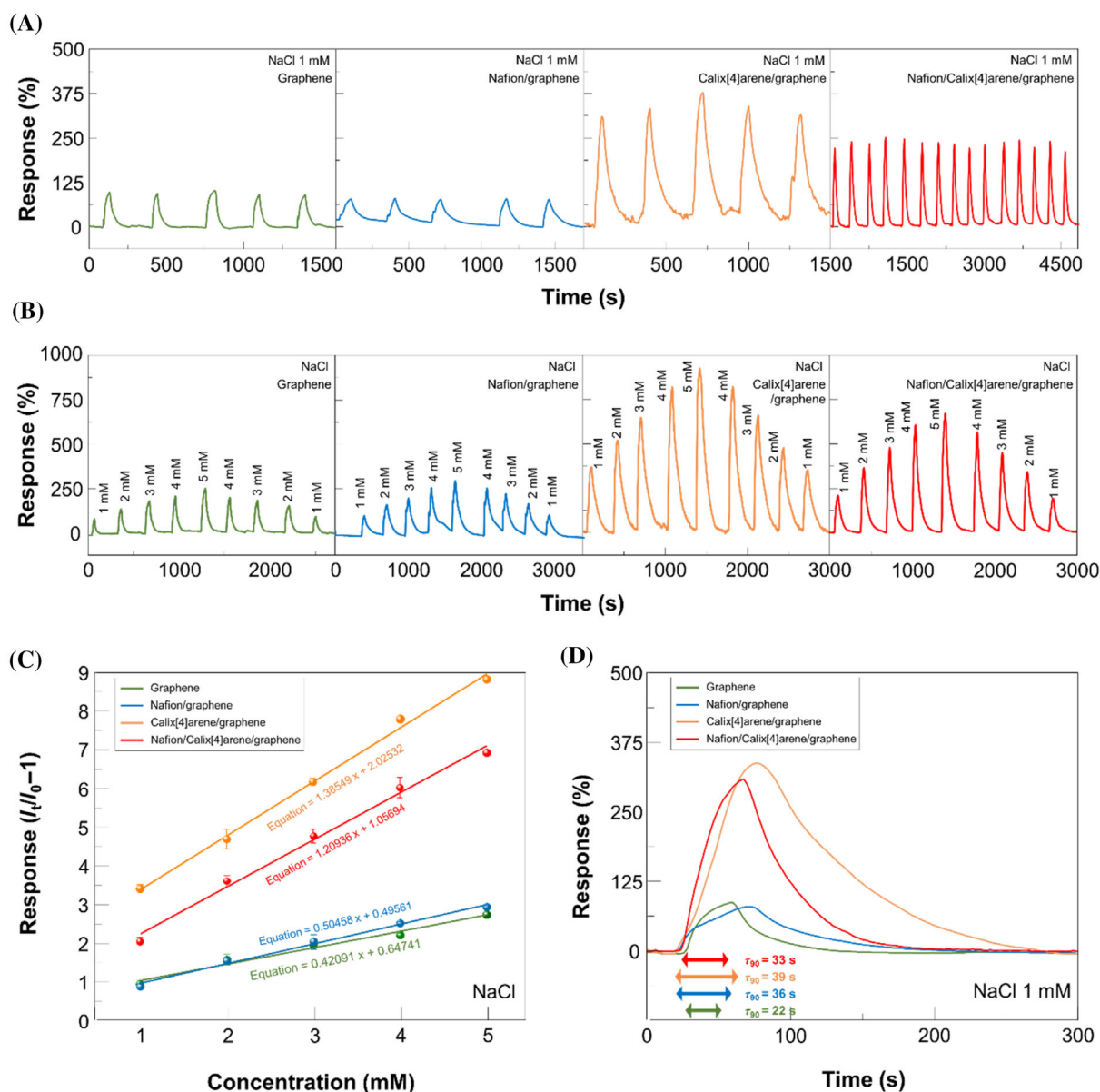
FIGURE 3 Na$^+$ detection characteristics of graphene, Nafion/graphene, Calix[4]arene/graphene, and Nafion/Calix[4]arene/graphene. (A) Na$^+$ responses (1–5 mM NaCl solutions) of the graphene SFETs. (B) Repetitive test of the graphene SFETs using 1 mM NaCl solution. (C) Linearity of the graphene SFETs by Na$^+$ concentration versus response. (D) The τ_{90} values of response to 1 mM NaCl of the graphene SFETs.

V_g induces a higher level of electron accumulation into the channel (n-type channel).[14] Eventually, the more the I_{ds}–V_g curve shifts to the left, the higher the n-type doping level. This is also evidence of not Cl$^-$ but Na$^+$ is the reacting agent with the surface of the graphene. If Cl$^-$ is the reacting factor with graphene, the graphene becomes p-doped, and the transfer curves should move to the opposite of the results. Other studies show an opposite Dirac point shift (right shift) when an anion approaches or hole doping occurs on the surface.[6,54,55]

Figure 3A displays a repetitive test of 1 mM NaCl of the four graphene SFETs. Especially, Na$^+$ detection of

Nafion/Calix[4]arene/graphene was conducted 10 times more than the rest of the samples to reveal the stability of the fabricated device. All samples have consistent responses but are differentiated by the degree of sensitivity. Figure 3B displays responses to a gradual increase in the concentration of Na$^+$ of the four different samples. The four samples show reversibility and reliability from repetitive responses to the same concentration without influencing the previous injected solution. This indicates the fabricated device is reliable and applicable as a Na$^+$ sensor.

The Nafion membrane acts as an ionic/molecular sieve preventing large ions or molecules from passing

through to enhance selectivity. Smaller ions that can penetrate through the membrane hinder perfect selective detection; a receptor is crucial. CVD graphene and Nafion/graphene have similar responses of Na^+, H^+, citric acid, KCl, $CaCl_2$, $MgCl_2$, NH_4Cl, and glutamic acid shown in Figure 3A,B and Figures S4a–l, S5a,b, S6a–l, and S7a,b, which can be inferred that Nafion allows small ions or molecules to penetrate. However, this membrane discrete large ions/molecules, and the surface of graphene increases selectivity, as displayed in Figures S5c–h and S7c–h. The responses to glucose, uric acid, and ascorbic acid are compared. It can be inferred that Nafion coating prevents glucose, uric acid, and ascorbic acid from penetrating through the sieve.

The introduction of the receptor is vital to distinct minuscule ions and molecules. Other research has shown Calix[4]arene as a well-performed receptor of Na^+.[29–31] In Figure 3A,B, the response to Na^+ of Calix[4]arene/graphene and Nafion/Calix[4]arene/graphene are enhanced than graphene and Nafion/graphene. From the results, it is assumed that Calix[4]arene helps the adhesion of Na^+ to the surface of the graphene. Also, comparing the response results of Na^+ and other ions shown in Figure 3A,B and Figures S4a–l, S5a–h, S8a–l, and S9a–h refer to Calix[4]arene assists most for Na^+ rather than other ions or molecules. The response ratio estimation of all ions and molecules between the samples is depicted below. Figure 3C displays the linear relationship between the concentration and response to Na^+ of all four graphene SFETs. The slope of graphene, Nafion/graphene, Calix[4]arene/graphene, and Nafion/Calix[4]arene/graphene are similar, respectively. The existence of the receptor provides a difference in the slope showing the response degree between concentrations becomes larger. The slopes of CVD graphene, Nafion/graphene, Calix[4]arene/graphene, and Nafion/Calix[4]arene/graphene are 0.42091 $(mM)^{-1}$, 0.50458 $(mM)^{-1}$, 1.38549 $(mM)^{-1}$, and 1.20936 $(mM)^{-1}$, respectively. The response time was also estimated by evaluating the time to reach 90% saturation after applying the target material depicted in Figure 3D. The time to reach the 90% saturation point is represented by τ_{90}. The values of τ_{90} for CVD graphene was 22 s, Nafion/graphene was 36 s, Calix[4]arene/graphene was 39 s, and Nafion/Calix[4]arene/graphene was 33 s.

2.3 | Long-term stability, detection limit, and selectivity of the graphene SFETs

To investigate the properties of a sensor, not only selectivity and sensitivity issues but also long-term stability, detection limit, and transfer characteristics are crucial factors. Figure 4A shows the repetitive responses of the fabricated device from Figure 3A after 220 days. Both samples show similar sensitivity and stability, assuming the device is usable after a long time. Figure 4B,C depicts the detection limit of graphene and Nafion/Calix[4]arene/graphene, respectively. The solutions were 100 nM, 1 μM, 10 μM, 100 μM, 1 mM, and 10 mM of NaCl. Graphene showed indistinguishable responses to 100 nM, 1 μM, and 10 μM, and the sensitivity increase of 100 μM was insignificant. It can be assumed that graphene has a low detection limit and would be positioned between 100 and 10 μM. On the other hand, the response to all solution concentrations of Nafion/Calix[4]arene/graphene was distinguished by having a high detection limit. Also, the response to 1 mM NaCl solution of graphene and Nafion/Calix[4]arene/graphene matches the response from Figure 3A. In the 10 mM NaCl solution, Nafion/Calix[4]arene/graphene shows a significant response elevation compared to graphene. Figure 4D,E depicts the response to all ions and molecules of graphene, Nafion/graphene and Calix[4]arene/graphene, Nafion/Calix[4]arene/graphene, respectively. As shown in Figure 4D, graphene and Nafion/graphene have identical responses to small ions or molecules that permeate the Nafion membrane. On the other hand, glucose, uric acid, and ascorbic acid have no response to Nafion/graphene, which cannot pass through the membrane. Figure 4E also has a similar tendency to Figure 4D in glucose, uric acid, and ascorbic acid cases. According to Figure 4D,E, responses of other ions and molecules slightly decrease when the Nafion membrane exists. This can be assumed that the presence of a sieve might slightly slower the reaction between the molecules and ions than direct contact. However, the response decline rate is negligible and banning larger ions and molecules is much more advantageous. Additionally, the Nafion film assists the graphene in preventing degradation and physically sweeping away from the solutions. This is assumed from the long-term stability having consistent detection signals after 220 days. Figure 4F depicts the response ratio between graphene and Nafion/Calix[4]arene/graphene of all ions and molecules. The response values were obtained from Figure 3A,B and Figures S4a–l, S5a–h, S10a–l, and S11a–h. Na^+ has the highest response ratio, meaning Na^+ is the most selective among the ions/molecules. The response of H^+ (H_3O^+) or citric acid has a higher absolute value than Na^+ in all four samples due to the high reaction between the ions and the surface of the graphene.[56] Nevertheless, the response values of graphene, Nafion/graphene, Calix[4]arene/graphene, and Nafion/Calix[4]arene/graphene of H^+ or citric acid are almost identical. This leads to the fact that Calix[4]arene is unrelated to H^+ or citric acid and eventually reveals a low ratio when divided by response values. To prove the
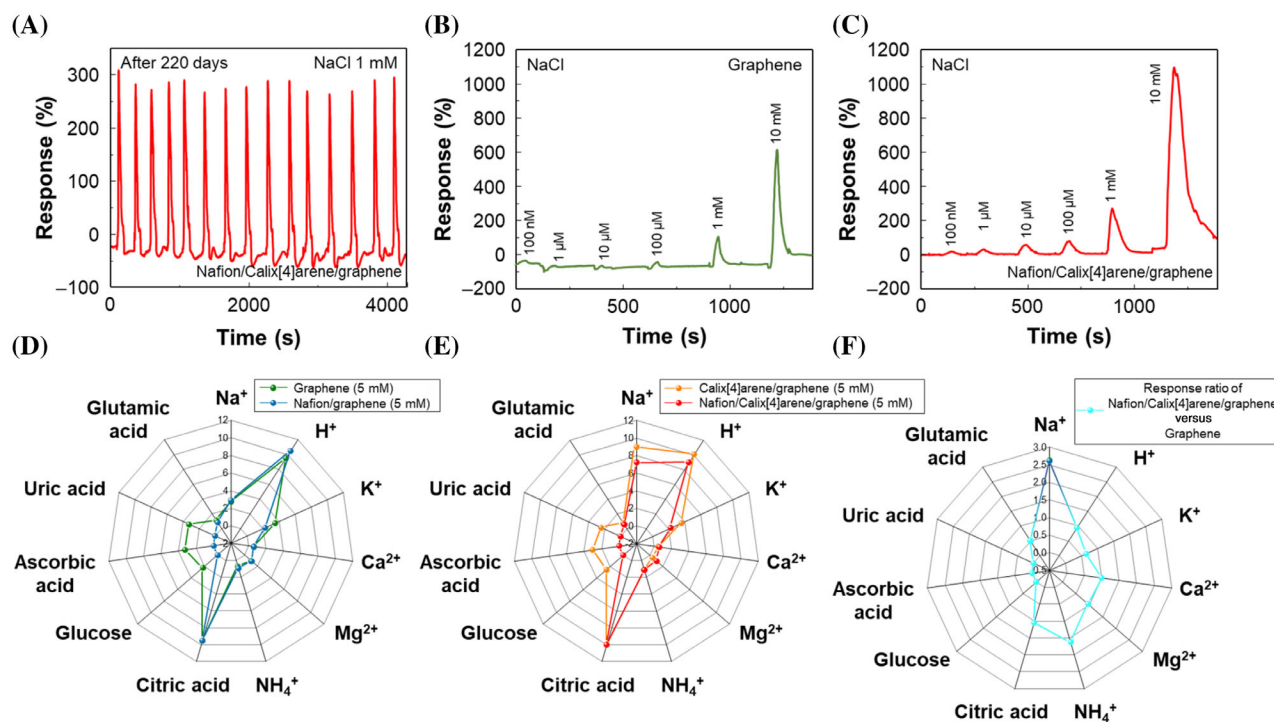
FIGURE 4 Long-term stability, detection limit, selectivity of Calix[4]arene/Nafion decorated graphene to Na⁺. (A) Long-term stability measurements using the identical sample from Figure 3 after 220 days. (B) Detection limit measurements of CVD graphene. (C) Detection limit measurements of Calix[4]arene/Nafion decorated graphene. (D) Responses of CVD graphene and Nafion coated graphene to various 5 mM concentrated ions/molecules. (E) Responses of Calix[4]arene decorated graphene and Calix[4]arene/Nafion decorated graphene to various 5 mM concentrated ions/molecules. (F) Ratio between the responses of Calix[4]arene decorated graphene and CVD graphene to scrutinize selectivity.

uniformity of the Nafion/Calix[4]arene/graphene device, another device was fabricated with the identical method, and then responses of 1 mM NaCl were evaluated. (Figure S12a) Then, the responses of 1 mM NaCl were collected from Figures 3A and 4A, and Figure S12a and plotted in a normal distribution bell curve (Figure S12b). All responses were included in the confidence interval of 95%, which can be understood as having uniformity of the device. For further stability issues, the device used from Figure 4A was evaluated with responses of 1 mM NaCl which have passed 868 days since the initial measurements (Figure S12c).

2.4 | Microcontroller unit device integration for further applications evaluating real beverages and detection mechanisms

In addition to measurements using chemical solutions, real beverages were also examined to evaluate the potential of practical applications of the fabricated device. The Nafion/Calix[4]arene/graphene SFET was also integrated with an MCU device to determine salinity for further

applications. The conducted MCU integrated device is illustrated in Figure 5A–E. Figure 5A is the scheme of the overall MCU device, including the micropipette for injection of the solutions (Figure 5B), microfluidic channel integrated Nafion/Calix[4]arene/graphene device (Figure 5C), MCU device on a breadboard with LEDs and resistors (Figure 5D), and a mobile phone having remote notification by the application in wi-fi conditions. (Figure 5E) The tests were held with 1, 5, and 10 mM of NaCl, each having a different remote signal from the MCU device and the mobile phone application. First, clean water is injected before the salinity test. When DI passes, none of the LEDs turn on, and the mobile phone shows a signal output "No salt, Clean water" (Figure S13a). Once 1 mM NaCl passes through the SFET, the yellow LED lights up while the blue LED is kept off, and the mobile phone gives a signal output "Too bland" (Figure S13b) 5 mM NaCl causes the blue LED to be turned on while the yellow being kept off and the mobile phone shows "Moderate" on the screen (Figure S13c). Finally, when 10 mM NaCl flows in, both LEDs turn on, and the screen reveals "Too salty" on the screen. (Figure S13d) The overall process of injecting solutions in the sequence of DI, 1 mM NaCl, DI, 5 mM
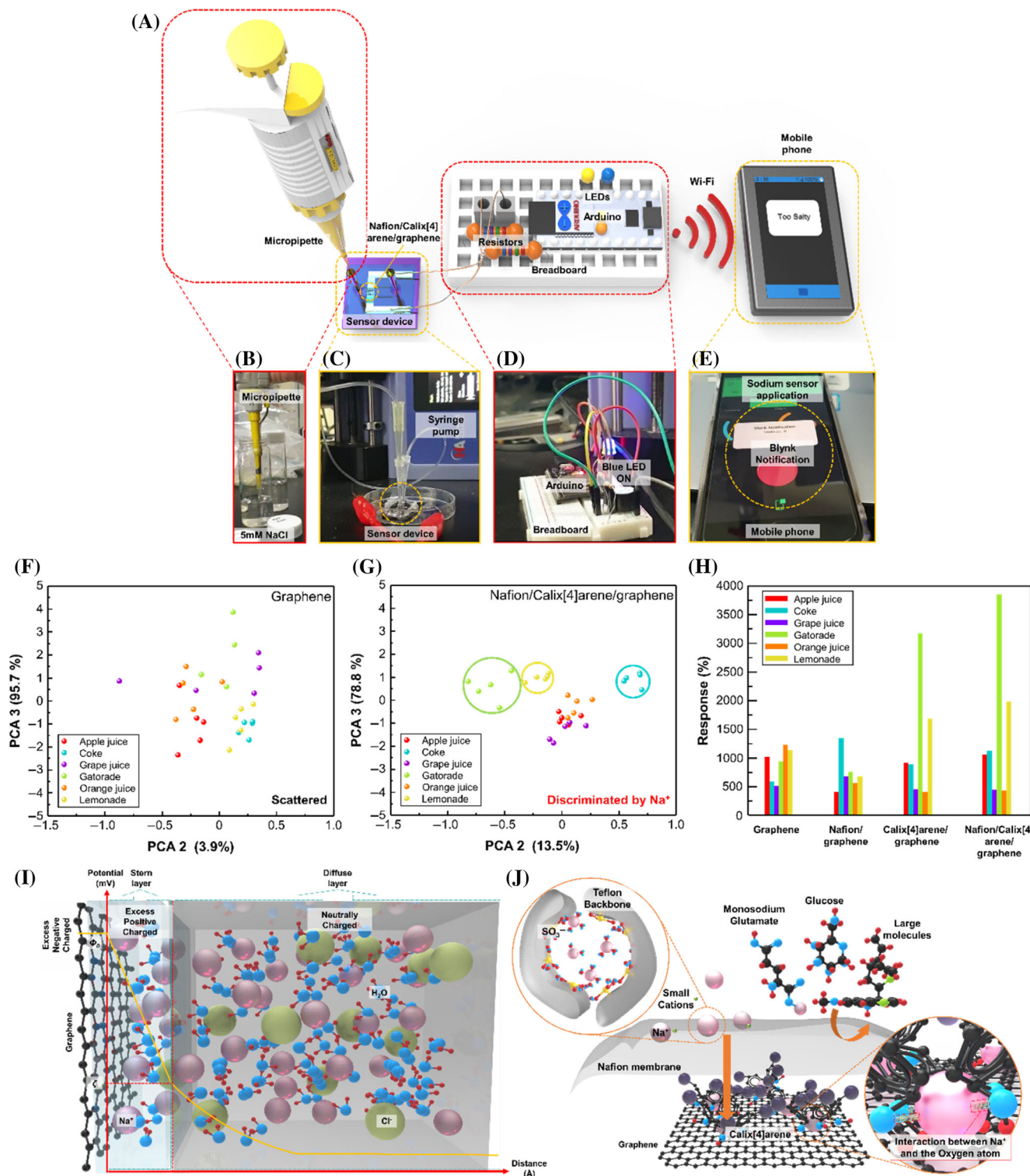
LEE ET AL.

FIGURE 5 MCU integrated to the fabricated device and mobile phone for applications, PCA plots and responses to real beverages of the four types of SFETs, and detection mechanism of the CVD graphene and Calix[4]arene/Nafion decorated graphene to Na$^+$. (A) Overall scheme of the integrated MCU and device with a mobile phone for remote notification. (B) Real image of the micropipette and NaCl solution. (C) Image of the device. (D) Magnified image of MCU and LED light. (E) Mobile phone and the sodium sensor application using an application. (F) PCA plots of pristine graphene. (G) PCA plots of Calix[4]arene/Nafion decorated graphene. (H) Response bar chart of the four types of SFETs to apple juice, coke, grape juice, Gatorade, orange juice, and lemonade. (I) Scheme of the Na$^+$ adsorption mechanism of graphene forming an Electric double layer (EDL). (J) Scheme of the overall Na$^+$ detection mechanism of Calix[4]arene/Nafion decorated graphene.

NaCl, DI, 10 mM NaCl, and DI is recorded and can be viewed in Video S1. Also, the processing methods and procedures are introduced in Figure S13e.

The beverages were apple juice, coke, grape juice, Gatorade, orange juice, and lemonade. All six beverages were estimated with graphene, Nafion/graphene, Calix[4]arene/graphene, and Nafion/Calix[4]arene/graphene. The repetitive response measurements are plotted in Figures S14–S17. For a more conspicuous comparison of the beverages between these four graphene-based SFETs, principal component analysis (PCA) was conducted, as shown in Figure 5F,G and Figure S18a,b. The variables were response time, sensitivity, and recovery time. The data loss was ignorable by neglecting one variable, "response time", for every four graphene-based samples, indicating that the PCA data are reliable. The PCA plots between graphene and Nafion/Calix[4]arene/graphene are differentiated by the dispersion of the data. The plots from the same beverage must be adjacent, while different beverage plots must be positioned far away. From this perspective, graphene plots are randomly scattered, having no order. (Figure 5F) Meanwhile, the plots from different beverages of Nafion/Calix[4]arene/graphene are spread out, and identical beverages are gathered. (Figure 5G) Especially, as depicted in Table S1, Gatorade has the highest concentration of Na^+, which is assumed to be differentiated most in the PCA plot. Classifying the beverages in terms of the nutrition facts, especially the amount of Na^+ (Table S1), apple juice, orange juice, and grape juice are relatively similar to each other than Gatorade, lemonade, and coke. This coincides with Figure 5G, that which Gatorade is most separated from the medium while apple, grape, and orange juice, possessing relatively similar nutrition components, are gathered together. The PCA plots offer the reliability of the Nafion/Calix[4]arene/graphene SFET by real beverage evaluation and can be a milestone in developing E-tongue. The response values were depicted in Figure 5H, in which the average of the responses was calculated from the peaks of Figures S14–S17. Figure 5H shows that Gatorade has the highest response, which coincides with the PCA (Figure 5G) and nutrition facts of Gatorade (Table S1). As shown, the facilely designed graphene-based device has the capacity to discriminate various real beverages that include Na^+, which corresponds to the state-of-the-art research using low dimensional nanoscale materials for sensor applications[57,58] or detecting Na^+.[59]

The detection mechanism is illustrated in Figure 5I,J. First, Figure 5J shows that Na^+ or other cations and large molecules approach the Nafion membrane; only Na^+ or other cations can permeate the sieve due to the unique ionic transfer mechanism of Nafion. When cations transfer through Nafion, two representative mechanisms exist for an explanation. Usually, H^+ hops through the membrane by combining with H_2O molecules to form an H_3O^+ and move on to the adjacent H_2O molecule. This mechanism is called the Grotthus method. On the other hand, cations rather than protons, such as Li^+, Na^+, and so on, diffuses in a different method called the vehicle-type mechanism. This transfer method is the direct migration of protons moving through the medium with a proton solvent like H_3O^+.[60]

Once Na^+ penetrates the Nafion sieve, the Na^+ ions interact with the surface of the graphene, and Calix[4]arene captures them selectively. The Na^+ and graphene have physisorption forming a bond between each other.[61] Cl^- ions are repulsive to the surface of the graphene due to negative adsorption energy.[62,63] Na^+ ions are attracted to the surface and positioned at the Stern layer. In contrast, Cl^- ions are located at the diffuse layer forming an electrical double layer (EDL) as depicted in Figure 5I.[64,65] This corresponds to the fact that the graphene becomes n-doped (electrons allocated to the upper surface of the graphene) as NaCl solutions were injected from the results in Figure 2A–D. According to the Gouy–Chapman–Stern model for the EDL, the Na^+ ions adsorb onto the graphene surface. However, their sizes are finite, causing them to be positioned some distance δ away from the surface compared to the Gouy–Chapman theory, which assumes the approaching ions as point charges and has no physical limits for them to become adjacent to the surface, which is incorrect. This distance is assumed to be the radius of the cation; in this case, Na^+. As the distance becomes further from the graphene surface, the potential drops linearly in the first place and then drops exponentially through the diffuse layer.[64]

As the Na^+ adsorbs to the surface of the graphene, the charge density at the gate electrode alters. As a result, the ionic charges at the surface of the graphene change the conductivity of the channel and induce an electrical sensing signal detected by an instrument.

It is well known that Calix[4]arene selectively captures various cations[29,30] but especially has higher selectivity for Na^+ over others such as Li^+, K^+ which corresponds with the sensing results shown in Figure 3A,B and Figure S8e,f.[29] This is due to the interaction between Na^+ and the oxygen-rich region of Calix[4]arene shown in Figure 5J while Li^+, K^+ interact with the *tert*-butyl groups of the macrocycle (which are absent from Calix[4]arene used in this study), indicating the reaction site differs from each other.[29] To conclude, the high response signal of Calix[4]arene/graphene or Nafion/Calix[4]arene/graphene to Na^+ is from the synergetic effect of both graphene and Calix[4]arene selectively and sensitively attracting Na^+, and this is proved by comparing other researches based on detecting Na^+ without

TABLE 1 Comparison of other contemporary researches based on Na^+ detection.

Channel material	Na^+ detection range	Measurement method	Response/ recovery time	Reversibility (amperometric)	Sensitivity	References
Fluorinated graphene	0.1 mM–1 M	Transfer curves, amperometric	~120 s, N/A	Irreversible	−55.4 mV dec^{-1}	66
Silicon nanowire	0.1 mM–1 M	Transfer curves, amperometric	~90 s, N/A	Reversible	59.16 mV dec^{-1}	67
Au-coated silicon nanowire	1 mM–1 M	Threshold voltage change by molarity	N/A, N/A	N/A	−44 mV dec^{-1}	68
Fluoropolysiloxane	0.01 mM–1 M	Amperometric	50 s, N/A	Irreversible	57 mV dec^{-1}	69
Amorphous In-Ga-Zn-oxide	1 mM–1 M	Amperometric	N/A, N/A	Reversible	60 mV dec^{-1}	70
Carbon black/ silicone elastomer composite	0.1 mM–1 M	Amperometric	~60 s, N/A	Reversible	56.1 mV dec^{-1}	71
Nafion/Calix[4] arene/graphene	100 nM–10 mM	Transfer curves, on–off available sensing curves	33 s, ~100 s	Reversible	5 mM: 690%	Our work

using Calix[4]arene/graphene of the fabricated device in Table 1.

3 | CONCLUSION

A novel ion/molecule graphene-based SFET was successfully demonstrated, which could selectively and sensitively detect Na^+ by a simple process for each step. To enhance the selectivity and sensitivity of the device, Nafion (molecular sieve) and Calix[4]arene (receptor) were coated or decorated on graphene. The Nafion film prevents large molecules from penetrating, allowing only Na^+ or small cations to pass, eventually increasing selectivity. Also, Calix[4]arene was decorated in a one-step method onto graphene to capture Na^+ more selectively and sensitively. The surface-tailored graphene SFET was integrated into a PDMS microfluidic channel, having the advantages of "real-time" and "dynamic" evaluation of ions or molecules. Not only limited to chemical species, real beverages, such as apple juice, coke, grape juice, Gatorade, orange juice, and lemonade, were tested with the fabricated graphene-based SFETs for practical applications. These beverages were successfully differentiated by PCA plotting. In addition, the fabricated graphene-based SFET was merged with an MCU device to estimate the salinity in a feasible method. The mobile phone and MCU device give an output signal that can be noticed immediately. A novel measurement and device fabrication method was introduced to detect particular ions or molecules. 2D materials possess high sensitivity but low selectivity to ions or molecules; we presented an advanced method enhancing both selectivity and sensitivity to detect Na^+. The device has the capacity to reliably discrete Na^+ from other ions or molecules and differentiates real beverages that consist of more Na^+ than others. These aspects of the device establish a milestone for implementing a practical E-tongue.

4 | EXPERIMENTAL SECTION

4.1 | Device preparation

The IDEs were produced by patterning using photolithography and depositing Pt/Ti (thickness of 100/30 nm) on SiO_2/Si substrates (SiO_2 thickness of 300 nm) by an e-beam evaporator. The patterned electrodes were designed with a size of 1 mm × 1 mm and a distance of 5 μm. After the patterning process, the IDE substrates were cleaned with acetone and isopropanol (IPA) via sonication for 20 min, then dried in N_2 gas.

The graphene samples were synthesized using CVD by CH_4 and H_2 gas, grown on a 25 μm-thick Cu foil in a quartz tube furnace system.[72] The furnace was heated in vacuum conditions of 90 mTorr. Before the growth process, Cu foil was preheated at 950°C for 30 min. To obtain a large, single-crystal Cu surface, H_2 gas at 35 sccm flowed in the furnace under 150 mTorr. After preheating, a mixture of CH_4 and H_2 gas at a ratio of 100:35 was

flowed in at ambient conditions for 10 min to synthesize the graphene. The furnace was cooled down quickly to room temperature (RT, 25°C) at 35 sccm H_2 gas flow after 10 min of graphene growth.

Following graphene growth, poly[methyl methacrylate] (PMMA, 46 mg mL^{-1} in chlorobenzene) was spin-coated on the graphene grown Cu foil. Then the baking process was conducted at 180°C for 1 min. Next, the other side of the Cu foil was treated with O_2 plasma to etch the graphene on the opposite side. Next, the sample was immersed in ferric chloride (1 M $FeCl_3$) bath at RT for longer than 12 h to etch away the Cu foil. Finally, the PMMA-coated graphene on the Cu foil was carefully dipped into DI more than 7 times to remove any remaining etchant. The PMMA-coated graphene was then carefully transferred onto the IDE. After the PMMA-graphene layer adhered to the IDE, the PMMA was removed by immersing the substrates at 70°C in acetone for 15 min and then cleaned with IPA and DI thoroughly.

The graphene-based SFETs were designed into four different groups; graphene, Nafion/graphene, Calix[4] aren/graphene, and Nafion/Calix[4]arene/graphene. Graphene had no more process on the surface compared with the others. Nafion/graphene was fabricated by spin-coating Nafion 117® on the graphene. Exactly, 0.1 mL of the Nafion 117® solution was dropped on the substrate and then spin-coated at the rate of 2000 rpm for 30 s. Before spin-coating, the source and drain electrodes were masked with tape to prevent contamination. After the spin-coating process, the Nafion/graphene samples were dried at 50°C for 30 min. Calix[4]arene decorated samples were fabricated by drop-casting 5 mM of Calix[4] arene dispersed in 5 mM *N,N*-dimethylmethanamide. Two micro liter of Calix[4]arene dispersed DMF solution was dropped onto the graphene 10 times and was dried for 3 min in between each drop to cover the surface of the graphene completely. Nafion/Calix[4]arene/graphene was fabricated by drop-casting Calix[4]arene and spin-coating Nafion as mentioned above. The four different samples were integrated with the patterned microfluidic channel for the measurements.

A 4-in. SiO_2/Si wafer was cleaned with acetone and then IPA via sonication for 20 min and dried with N_2 gas to form a patterned substrate for production of the microfluidic channel. The adhesion layer was created by spin-coating SU-8 2 on the wafer at 3000 rpm for 30 s. Then the soft baking process was performed at 65°C for 2 min and 95°C for 2 min in order. After the soft baking process, UV was exposed for 2 min using the UV lamp. Finally, the hard baking process was conducted at 180°C for 3 min. SU-8 50 was spin-coated for 3 min at 2000 rpm for the photoresist (PR) layer. UV exposure was

proceeded for 30 s, followed by hard baking at 180°C for 3 min. Developing was done for 3 min, rinsing with DI, and then drying with N_2 gas.

The microfluidic channel graphene-based SFET device was conducted by adhering the channel patterned PDMS onto the four graphene samples. Conventional PDMS replica molding technique was used to produce the channel patterned PDMS. A SU-82075 (Microchem Corp.) master template having a thickness of 100 μm and a width of 500, 800, and 1000 μm was used as a mold by conventional photolithography. The PDMS monomer and curing agent were mixed in the weight ratio of 10:1 (Sylgard 184) and were poured onto the SU-8 master template and then degassed in a vacuum chamber. The curing process was held for 1 h at 80°C, and the patterned microfluidic channel was cut with a razor and detached. To stabilize the adhesion between the IDE and channel patterned PDMS, the PDMS with acrylic transfer tape (Samchun chemicals) was exposed to O_2 plasma with a plasma power of 125 W, 120 s, and flow rate of O_2 at 60 sccm. The Cu wires were placed on the source, drain electrodes on the IDE, and PDMS were attached.

4.2 | Characterization, material preparation, and ion/molecule measurements

The thickness of the Nafion spin-coated samples was estimated using field-emission scanning electron microscopy (FESEM) (Merlin Compact), with an acceleration voltage of 5 kV and a working distance of 8.8 mm. The morphologies of the graphene were characterized using field-emission TEM (JEM-2100F, JEOL). Bright-field and high-resolution (HR) images were obtained by TEM. Raman spectroscopy (LabRAM HR Evolution) was used to prove the existence of graphene, Calix[4]arene, and the reception abilities of Calix[4]arene. X-ray photoelectron emission spectroscopy (Versaprobe III) were carried out to verify the existence of Calix[4]arene onto the surface of graphene. Fourier transform infrared (Nicolet iS50) spectra measurements were carried out to verify the existence of Calix[4]arene.

The NaCl solutions were obtained by dissolving NaCl powders (Daejung, 99.5%) in DI to obtain solutions with concentrations of 100 nM–10 mM solutions. HCl (Daejung, 35.4%) solutions were diluted to produce 1–5 mM concentrations. KCl powder (Daejung, 99%), $CaCl_2$ (Sigma Aldrich, 97%), $MgCl_2$ (Sigma Aldrich, 98%), NH_4Cl (Junsei, 99.5%), citric acid (Daejung, 99.5%), glutamic acid (Sigma Aldrich, 99%) was also dissolved to produce 1–5 mM solutions. Glucose (Sigma Aldrich, 99.5%), Uric acid (Sigma Aldrich, 99%), and L(+)

Ascorbic acid (Junsei, 99.6%) were dissolved into NaOH and produced 1–5 mM concentrated solutions. The NaOH solution was prepared by dissolving NaOH beads (Daejung, 97%) in DI, with a concentration of 0.1 M. The beverages for estimation were apple juice, coke, grape juice, Gatorade, orange juice, and lemonade. The nutrition facts are shown in Table S1. Coke is a carbonated beverage having bubbles that influence the device and electrical signals that produce noises. It was poured into a vial and sealed with parafilm. Then, the cover was punched with holes and left on a hot plate at about 60°C to release carbonic acid gas thoroughly from the drink. The Calix[4]arene ($C_{28}H_{24}O_4$) powders were purchased from TCI (Tokyo Chemical Industry, >98%). The Nafion 117® solution was purchased from Sigma-Aldrich.

Two syringe pumps (Pump 11 Elite Infusion/Withdrawal Programmable Dual Syringe) were used for the base solution injection and withdrawal. The flow velocity was 0.07 mL min^{-1}, and the infusion pump was paused when the target solution was injected using a micropipette (100 μL). (withdrawal pump kept running) The infusion pump was resumed for 100 s and paused until the depth of the solution returned and operated for 200 s until the next solution injection. The cycle repeat of each solution was 300 s. A Pt wire was inserted through the hole and contacted with a gate source. The electrical properties of the device were evaluated using an Agilent 4156C semiconductor analyzer with a source-drain voltage of 0.1 V and a gate voltage of −0.2 V.

The response of the sensing device is defined as follows:

$$\text{Response}\,(\%) = \frac{I_t - I_0}{I_0} \times 100\% = \frac{\Delta I}{I_0} \times 100\% \quad (1)$$

where I_t and I_0, respectively represent the electrical conductivity of the sensor in the presence of the target solution and base solution, respectively.

PCA was conducted by standardizing the data from the response of the beverages. From four different graphene-based SFETs, there were six beverages and five curves each. First, a matrix (A) is conducted by estimating the response time, sensitivity, and recovery time of all beverages from graphene. The matrix (A) would be 3 × 30 (rows are the variables and columns are the values of each variable) and conduct a matrix (B) that the components are the average value of each row. Then, subtract the matrix (A–B = C) from each other and transpose the matrix (C^T). After producing $C \times C^T$, multiply 29 (= 30−1) on the components (matrix D). Calculate the covariance matrix of D and then calculate the eigenvectors and eigenvalues for the covariant matrix. Since there were three variables, there are three eigenvalues which

are PCA 1 (response time), PCA 2 (sensitivity), and PCA 3 (recovery time). The larger two eigenvalues are the new x- and y-axis. Produce a new 3 × 3 matrix (E) whose components are the eigenvectors of the two large eigenvalues and the residue components as 0. Next, conduct a new matrix (F) by multiplying 29 on matrix C and transposing. Finally, multiply matrix F (30 × 3) and E (3 × 3), which are the plots of the new x and y-axis.

CONFLICT OF INTEREST STATEMENT
The authors declare no conflict of interest.

DATA AVAILABILITY STATEMENT
The data that support the findings of this study are available from the corresponding author upon reasonable request.

ORCID
Ho Won Jang https://orcid.org/0000-0002-6952-7359

REFERENCES
1. Hunter RW, Dhaun N, Bailey MA. The impact of excessive salt intake on human health. *Nat Rev Nephrol*. 2022;18(5):1-15.
2. Palmer BF, Gates JR, Lader M. Causes and management of hyponatremia. *Ann Pharmacother*. 2003;37(11):1694-1702.
3. Mastroianni B. Cooking at home more during COVID-19? What to know about food safety. Accessed August, 2020. https://www.healthline.com/health-news/cooking-at-home-more-during-covid-19-what-to-know-about-food-safety
4. World Health Organization. *Global Action Plan for the Prevention and Control of Noncommunicable Diseases 2013–2020*. World Health Organization; 2013.
5. Riul A Jr, Dantas CA, Miyazaki CM, Oliveira ON Jr. Recent advances in electronic tongues. *Analyst*. 2010;135(10):2481-2495.
6. Lee CW, Suh JM, Choi S, et al. Surface-tailored graphene channels. *npj 2D Mater Appl*. 2021;5(1):1-13.
7. Lvova L, Martinelli E, Mazzone E, et al. Electronic tongue based on an array of metallic potentiometric sensors. *Talanta*. 2006;70(4):833-839.
8. Habara M, Ikezaki H, Toko K. Study of sweet taste evaluation using taste sensor with lipid/polymer membranes. *Biosens Bioelectron*. 2004;19(12):1559-1563.

9. Riul A Jr, Malmegrim R, Fonseca F, Mattoso L. An artificial taste sensor based on conducting polymers. *Biosens Bioelectron*. 2003;18(11):1365-1369.

10. Lee CW, Suh JM, Jang HW. Chemical sensors based on two-dimensional (2D) materials for selective detection of ions and molecules in liquid. *Front Chem*. 2019;7:7.

11. Hasani A, Do HH, Tekalgne M, et al. Recent progress of two-dimensional materials and metal–organic framework-based taste sensors. *J Korean Ceram Soc*. 2020;57(4):353-367.

12. Suh JM, Shim YS, Kwon KC, et al. Pd- and Au-decorated MoS_2 gas sensors for enhanced selectivity. *Electron Mater Lett*. 2019;15(3):368-376.

13. Meric I, Han MY, Young AF, Ozyilmaz B, Kim P, Shepard KL. Current saturation in zero-bandgap, top-gated graphene field-effect transistors. *Nat Nanotechnol*. 2008;3(11):654-659.

14. Schwierz F. Graphene transistors. *Nat Nanotechnol*. 2010;5(7):487-496.

15. Salvo P, Melai B, Calisi N, et al. Graphene-based devices for measuring pH. *Sens Actuators B Chem*. 2018;256:976-991.

16. Maehashi K, Sofue Y, Okamoto S, Ohno Y, Inoue K, Matsumoto K. Selective ion sensors based on ionophore-modified graphene field-effect transistors. *Sens Actuators B Chem*. 2013;187:45-49.

17. Wang F, Liu L, Li WJ. Graphene-based glucose sensors: a brief review. *IEEE Trans Nanobioscience*. 2015;14(8):818-834.

18. Lei N, Li P, Xue W, Xu J. Simple graphene chemiresistors as pH sensors: fabrication and characterization. *Meas Sci Technol*. 2011;22(10):107002.

19. Ohno Y, Maehashi K, Yamashiro Y, Matsumoto K. Electrolyte-gated graphene field-effect transistors for detecting pH and protein adsorption. *Nano Lett*. 2009;9(9):3318-3322.

20. Lehmani A, Turq P, Périé M, Périé J, Simonin JP. Ion transport in Nafion® 117 membrane. *J Electroanal Chem*. 1997;428(1-2):81-89.

21. Stenina I, Sistat P, Rebrov A, Pourcelly G, Yaroslavtsev A. Ion mobility in Nafion-117 membranes. *Desalination*. 2004;170(1):49-57.

22. Chen Y, Zhu Z, Tian Y, Jiang L. Rational ion transport management mediated through membrane structures. *Explor*. 2021;1(2):20210101.

23. Diamond D, McKervey MA. Calixarene-based sensing agents. *Chem Soc Rev*. 1996;25(1):15-24.

24. Ludwig R, Dzung NTK. Calixarene-based molecules for cation recognition. *Sensors*. 2002;2(10):397-416.

25. Huang D, Song BY, Li MJ, Li XY. Oxygen diffusion in cation-form Nafion membrane of microbial fuel cells. *Electrochim Acta*. 2018;276:268-283.

26. Avci AH, Messana DA, Santoro S, et al. Energy harvesting from brines by reverse electrodialysis using Nafion membranes. *Membranes*. 2020;10(8):168.

27. Peng J, Lou K, Goenaga G, Zawodzinski T. Transport properties of perfluorosulfonate membranes ion exchanged with cations. *ACS Appl Mater Interfaces*. 2018;10(44):38418-38430.

28. Gutsche CD. Calixarenes. *Acc Chem Res*. 1983;16(5):161-170.

29. Rodriguez-Ropero F, Preat J, Zanuy D, Torras J, Aleman C. Sensing mechanism of calix[4]arene-substituted poly (thiophene) ion receptor: effects of the selectivity on the molecular rigidity. *J Phys Chem B*. 2009;113(24):8284-8287.

30. Marsella MJ, Newland RJ, Carroll PJ, Swager TM. Ionoresistivity as a highly sensitive sensory probe: investigations of polythiophenes functionalized with calix[4]arene-based ion receptors. *J Am Chem Soc*. 1995;117(39):9842-9848.

31. Crawford KB, Goldfinger MB, Swager TM. Na^+ specific emission changes in an ionophoric conjugated polymer. *J Am Chem Soc*. 1998;120(21):5187-5192.

32. Rummeli MH, Bachmatiuk A, Scott A, et al. Direct low-temperature nanographene CVD synthesis over a dielectric insulator. *ACS Nano*. 2010;4(7):4206-4210.

33. Passos RR, Paganin VA, Ticianelli EA. Studies of the performance of PEM fuel cell cathodes with the catalyst layer directly applied on Nafion membranes. *Electrochim Acta*. 2006;51(25):5239-5245.

34. Malard L, Pimenta MA, Dresselhaus G, Dresselhaus M. Raman spectroscopy in graphene. *Phys Rep*. 2009;473(5-6):51-87.

35. Hill W, Wehling B, Gibbs CG, Gutsche CD, Klockow D. Detection of aromatics in aqueous solution by surface-enhanced Raman scattering by substrates chemically modified with p-tert-butylcalix[4]arenetetrathiol. *Anal Chem*. 1995;67(18):3187-3192.

36. Bukola S, Liang Y, Korzeniewski C, Harris J, Creager S. Selective proton/deuteron transport through Nafion|graphene|Nafion sandwich structures at high current density. *J Am Chem Soc*. 2018;140(5):1743-1752.

37. Casiraghi C. Doping dependence of the Raman peaks intensity of graphene close to the Dirac point. *Phys Rev B*. 2009;80(23):233407.

38. Mukaddam M, Wang Y, Pinnau I. Structural, thermal, and gas-transport properties of Fe^{3+} ion-exchanged Nafion membranes. *ACS Omega*. 2018;3(7):7474-7482.

39. Gruger A, Régis A, Schmatko T, Colomban P. Nanostructure of Nafion® membranes at different states of hydration: an IR and Raman study. *Vib Spectrosc*. 2001;26(2):215-225.

40. Laporta M, Pegoraro M, Zanderighi L. Perfluorosulfonated membrane (Nafion): FT-IR study of the state of water with increasing humidity. *Phys Chem Chem Phys*. 1999;1(19):4619-4628.

41. Heitner-Wirguin C. Infra-red spectra of perfluorinated cation-exchanged membranes. *Polymer*. 1979;20(3):371-374.

42. Fan Y, Tongren D, Cornelius CJ. The role of a metal ion within Nafion upon its physical and gas transport properties. *Eur Polym J*. 2014;50:271-278.

43. Papagno M, Rusponi S, Sheverdyaeva PM, et al. Large band gap opening between graphene Dirac cones induced by Na adsorption onto an Ir superlattice. *ACS Nano*. 2012;6(1):199-204.

44. Jeon C, Shin HC, Song I, et al. Opening and reversible control of a wide energy gap in uniform monolayer graphene. *Sci Rep*. 2013;3(1):2725.

45. Sung SJ, Lee PR, Kim JG, Ryu MT, Park HM, Chung JW. Band gap engineering for graphene by using Na^+ ions. *Appl Phys Lett*. 2014;105(8):081605.

46. Ahn Y, Kim J, Ganorkar S, Kim YH, Kim SI. Thermal annealing of graphene to remove polymer residues. *Mater Express*. 2016;6(1):69-76.

47. Kim YH, Park JS, Choi YR, et al. Chemically fluorinated graphene oxide for room temperature ammonia detection at ppb levels. *J Mater Chem A*. 2017;5(36):19116-19125.

48. Chen X, Wang X, Fang D. A review on C1s XPS-spectra for some kinds of carbon materials. *Fuller Nanotub Carbon Nanostruct*. 2020;28(12):1048-1058.

49. Siokou A, Ravani F, Karakalos S, Frank O, Kalbac M, Galiotis C. Surface refinement and electronic properties of graphene layers grown on copper substrate: an XPS, UPS and EELS study. *Appl Surf Sci*. 2011;257(23):9785-9790.

50. Perrozzi F, Prezioso S, Donarelli M, et al. Use of optical contrast to estimate the degree of reduction of graphene oxide. *J Phys Chem C*. 2013;117(1):620-625.

51. Cooper AJ, Wilson NR, Kinloch IA, Dryfe RA. Single stage electrochemical exfoliation method for the production of few-layer graphene via intercalation of tetraalkylammonium cations. *Carbon*. 2014;66:340-350.

52. Wang Z, Xue Z, Zhang M, et al. Germanium-assisted direct growth of graphene on arbitrary dielectric substrates for heating devices. *Small*. 2017;13(28):1700929.

53. Mattiuzzi A, Jabin I, Mangeney C, et al. Electrografting of Calix[4]arenediazonium salts to form versatile robust platforms for spatially controlled surface functionalization. *Nat Commun*. 2012;3(1):1-8.

54. Ang PK, Chen W, Wee ATS, Loh KP. Solution-gated epitaxial graphene as pH sensor. *J Am Chem Soc*. 2008;130(44):14392-14393.

55. Schedin F, Morozov AK, Hill EW, Blake P, Katsnelson MI, Novoselov KS. Detection of individual gas molecules adsorbed on graphene. *Nat Mater*. 2007;6(9):652-655.

56. Cole DJ, Ang PK, Loh KP. Ion adsorption at the graphene/electrolyte interface. *J Phys Chem Lett*. 2011;2(14):1799-1803.

57. Yu L, Yi Y, Yao T, et al. All VN-graphene architecture derived self-powered wearable sensors for ultrasensitive health monitoring. *Nano Res*. 2019;12(2):331-338.

58. Li L, Zhao S, Ran W, et al. Dual sensing signal decoupling based on tellurium anisotropy for VR interaction and neuro-reflex system application. *Nat Commun*. 2022;13(1):5975.

59. Zhong B, Jiang K, Wang L. Wearable sweat loss measuring devices: from the role of sweat loss to advanced mechanisms and designs. *Adv Sci*. 2022;9(1):2103257.

60. Zuo Z, Fu Y, Manthriam A. Novel blend membranes based on acid-base interactions for fuel cells. *Polymers*. 2012;4(4):1627-1644.

61. Patra N, Esan DA, Kral P. Dynamics of ion binding to graphene nanostructures. *J Phys Chem C*. 2013;117(20):10750-10754.

62. Yin J, Li X, Yu J, Zhang Z, Zhou J, Guo W. Generating electricity by moving a droplet of ionic liquid along graphene. *Nat Nanotechnol*. 2014;9(5):378-383.

63. Yin J, Zhang Z, Li X, Zhou J, Guo W. Harvesting energy from water flow over graphene? *Nano Lett*. 2012;12(3):1736-1741.

64. Brown MA, Abbas Z, Kleibert A, et al. Determination of surface potential and electrical double-layer structure at the aqueous electrolyte-nanoparticle interface. *Phys Rev X*. 2016;6(1):011007.

65. Lee SA, Yang JW, Choi S, Jang HW. Nanoscale electrodeposition: dimension control and 3D conformality. *Explor*. 2021;1(3):20210012.

66. Oh HG, Jeon DC, Gianti MS, et al. Two−dimensional disposable graphene sensor to detect Na^+ ions. *Nanomater*. 2021;11(3):787.

67. Cho S, Cho WJ. Highly sensitive and selective sodium ion sensor based on silicon nanowire dual gate field-effect transistor. *Sensors*. 2021;21(12):4213.

68. Wipf M, Stoop R, Tarasov A, et al. Selective sodium sensing with gold-coated silicon nanowire field-effect transistors in a differential setup. *ACS Nano*. 2013;7(7):5978-5983.

69. Cazalé A, Sant W, Launay J, Ginot F, Temple-Boyer P. Study of field effect transistors for the sodium ion detection using fluoropolysiloxane-based sensitive layers. *Sens Actuators B*. 2013;177:515-521.

70. Ito K, Satake H, Mori Y, Tseng A, Sakata T. Biocompatible and Na^+-sensitive thin film transistor for biological fluid sensing. *Sci Technol Adv Mater*. 2019;20(1):917-926.

71. Lim HR, Kim YS, Kwon S, et al. Wireless, flexible, ion-selective electrode system for selective and repeatable detection of sodium. *Sensors*. 2020;20(11):3297.

72. Ci H, Chen J, Ma H, et al. Transfer-free quasi-suspended graphene grown on a Si wafer. *Adv Mater*. 2022;34(51):2206389.

SUPPORTING INFORMATION

Additional supporting information can be found online in the Supporting Information section at the end of this article.